



Contents lists available at ScienceDirect

International Journal of Disaster Risk Reduction

journal homepage: www.elsevier.com/locate/ijdrr



Risk-aware navigation in industrial plants at risk of NaTech accidents

Gerard J. O'Reilly ^{a,*}, Davit Shahnazaryan ^a, Paolo Dubini ^b, Emanuele Brunesi ^b, Annalisa Rosti ^b, Filippo Dacarro ^b, Alberto Gotti ^b, Davide Silvestri ^b, Sergio Mascetti ^c, Mattia Ducci ^c, Mariano Ciucci ^d, Alessandra Marino ^d

^a Scuola Universitaria Superiore IUSS Pavia, Pavia, Italy

^b European Centre for Training and Research in Earthquake Engineering (EUCENTRE), Pavia, Italy

^c Università Degli Studi di Milano, Milan, Italy

^d National Institute for Insurance Against Accidents at Work (INAIL)/DIT, Rome, Italy

ARTICLE INFO

Keywords:

Risk-aware navigation
Sensors
Industrial plants
Structural risk
Environmental risk

ABSTRACT

Industrial plants are susceptible to NaTech disasters during earthquakes caused by damage to structural and non-structural components and the potential release of toxic materials. To mitigate and manage this risk, the ROSSINI project was initiated and its results are described here for what concerns industrial plant worker safety and their risk-based navigation in emergency situations. The project includes a data acquisition system consisting of a data acquisition board and an array of different sensor technologies, which process the seismic event and other meteorological information before passing them as inputs towards the risk identification and evaluation (RIE) modules. Here, the risks associated with structural and non-structural damage and health risks associated with the release of harmful substances are estimated and combined to form a navigable risk map. This map is used within a purpose-built risk-based navigation application for the safe egress of workers from an industrial plant. To demonstrate the implementation of this system, two case-study industrial plant layouts consisting of buildings, non-structural components, liquid storage tanks, piping systems, and chemical storage vessels, were devised. This paper describes the project's implementation in these contexts and illustrates the results via several example scenarios.

1. Introduction

Accidents initiated by natural hazards like earthquakes that trigger technological disasters are termed NaTech accidents, as listed on the eNatech Database (<https://enatech.jrc.ec.europa.eu/>). When occurring in industrial plants, these events have a high potential for structural and non-structural element damage and collapse, in addition to the release of toxic substances into the local environment. Akin to many countries around the world, Italy is also susceptible to NaTech events, especially harmful to large important facilities like industrial plants consisting of numerous buildings and hazardous equipment, the failure of which could result in significant impacts on human health to the point of serious injury or death. Furthermore, many processes within the industrial facilities are conducted in series, meaning the failure of one component could halt the entire process resulting in business interruption. Over the years, substantial amounts of failures leading to casualties in industrial plants have been documented following seismic events [1], documented the destructive damage to industrial areas leading to long-term fires in petroleum refineries following the Niigata Earthquake

* Corresponding author.

E-mail address: gerard.oreilly@iusspavia.it (G.J. O'Reilly).

in 1964; damage to power stations, and lifelines following the Tokachi-Oki Earthquake in 1968; damage to piping and large tanks due to sloshing following the Miyagi Ken-Oki Earthquake in 1978, among others. The 1999 Izmit earthquake in Turkey caused significant damage to the Tupras refinery following the structural collapse of a concrete chimney, and the subsequent release of a large volume of toxic substances into the surrounding environment [2]. More recently, chemical facilities were severely damaged following the L'Aquila Earthquake in 2009. Three silos storing polypropylene beads were significantly damaged leading to collisions with an adjacent warehouse resulting in the partial crushing of concrete walls [3]. Furthermore, pipelines transferring gas were damaged, releasing substances, which albeit not harmful, are symptomatic of the potential hazard to life safety in ensuing earthquakes should dangerous substances be stored [4]. The above was confirmed by the Emilia-Romagna earthquake in Italy in 2012, indicating the high vulnerability of facilities accentuated by the risk of dangerous substances released into the local and surrounding environment because of pipelines rupturing or storage tanks failing. Additionally, the collapse of buildings within the plant area led to simultaneous damage of pipelines amplifying the implications of safety systems' failure through multiple accident chains [3]. highlights the implications of collapsing components and the subsequent release of toxic substances for human health potentially leading to death despite the moderate intensity of the earthquake, and hence must not be ignored.

The observed severity of failures in industrial facilities and potential health safety concerns necessitate the implementation of safety measures, such as passive control techniques for seismic protection, like base isolation or other dissipation systems [5,6]. Even though the implementation of such systems is of great importance, the safe egress of workers remains a priority. Therefore, within this study, a risk-aware navigation system was developed with the goal of managing and mitigating the seismic risk associated with human health in industrial plants following seismic events. The collaborative efforts of the Scuola Universitaria Superiore IUSS Pavia, the Eucentre Foundation, the University of Milan and the Italian National Institute for Insurance against Accidents at Work (INAIL) led to the design, implementation, and testing of a prototype system for integrated risk-aware navigation within industrial plants at risk of accidents following seismic events, entitled ROSSINI (Rischio SiSmico in industrie a rischio di INcidente rIlevante), which is described herein.

Within this study, the objectives of the ROSSINI project are illustrated along with the sensor technologies utilised. Its implementation is detailed with the use of a multi-sensor array for integrated risk computation in industrial plants at risk of NaTech accidents. A key part of the system involves the Risk Identification and Evaluation (RIE) modules, where the risk metrics associated with structural and non-structural failure are combined with the risks due to the release of dangerous substances into the local environment, potentially impacting human health. For a given seismic shaking detected at an industrial plant through the multi-sensor array, the system furnishes a real-time risk map for plant workers to use, and be navigated by, to exit through the safest (i.e., minimal risk) route automatically calculated by the system. Risks associated with the damage to elements such as piping systems, industrial structures, tanks, and storage vessels are combined with the probability of toxic substances being released and diffused into the local environment. Structural and non-structural failure risk estimates are based on a classic fragility function approach, where the probability of a given damage threshold, and subsequent consequence, are estimated from a database of collected fragility and consequence functions and relayed to plant workers via the risk map. For what concerns the environmental risk, atmospheric dispersion models are employed to simulate the accidental continuous, transient, instantaneous, or catastrophic release of chemicals, to predict air concentration levels of toxic substances in the surrounding environment. The latter are then compared against chemical-specific toxicological thresholds to assess the severity of the impacts on human health. Finally, the computational architecture developed for the identification of the safest exit route and its implementation within a mobile application is described. Using the tools developed, the system within the ROSSINI project is appraised via its application to case-study industrial plants considering ground shakings of various intensities and other potential scenarios.

2. Overview of the risk assessment framework

Estimation of the risk of casualties following an earthquake event requires knowledge of fragility models related to the collapse probability of structural and non-structural components within the industrial plant [7]. noted the relationship between the number of casualties after seismic events and the number of fully or partially collapsed buildings. Empirical fatality models have been developed over the years to account for the extent of the collapse. For example [8], developed a semi-empirical framework to estimate fatality and consequence models leading towards the computation of a risk metric termed "local personal risk" (LPR). The LPR is a combination of the probability of dying inside or outside a building given collapse, identifying the risk a building poses to a single person that is permanently located within or near a building. Similarly [9], discussed several fatality risk metrics, including individual risk, defined as the probability of an average unprotected person, permanently present at a certain location, being killed due to an accident resulting from a hazardous event. The existing literature is mainly focused on casualty estimation based on the direct collapse of structural and non-structural components, either using empirical or analytical models depending on the location of a person relative to the building.

[7] considered several factors, including the number of people inside the building at the time of seismic action, and the percentage of people trapped by collapse and unable to escape. In contrast [10], demonstrated the importance of potential casualties around the perimeter of the building because of falling debris. Therefore, an influence zone can be identified for components and buildings within the plant layout of the building. Additionally, instead of computing a probability of casualty based on relative probability dependent on inside or outside risk, a more direct risk is computed as the actual location of a person within the plant is known at any given time. To account for developments in past studies regarding consequence models, the navigation system described herein is assumed to be installed on a mobile device that each worker possesses and has an objective to estimate risk throughout the entirety of the industrial plant at any given time assuming a dynamically changing environment. The navigation system aims to devise a least-

risk path towards emergency exits based on combined risks due to structural and environmental impacts as described within Section 5.1 and Section 5.2, respectively. The RIE framework architecture utilised as a part of the ROSSINI project is illustrated schematically in Fig. 1 and is described in further detail in the following sections. Once an earthquake event is detected, the raw signal is processed through sensor technologies and propagated through the data acquisition board, where the ground motion intensity measures as well as other pertinent sensor data are passed to the RIE modules. Here, the RIE modules utilise the analytical database comprised of fragility and consequence functions and estimate damage and dispersions of toxic substances into the local environment. The analytical database is stored in the system while the computations of risks will be carried out and stored after each seismic event. Finally, the output of risks is passed to the navigation system, which maps the risks and provides the safest path for a given worker through the mobile app.

3. Sensor technologies

The platform utilised in ROSSINI integrates structural and environmental RIE modules. The risks associated with the structural damage of buildings and damageable plant components, such as pipelines, tanks and vessels, are estimated within the structural RIE module. The environmental RIE module instead is based on estimating the concentration field of chemicals in the industrial plant due to the release from plant components and simulating its spatial diffusion over time. The input data for both RIEs are implemented within the ROSSINI platform, which acquires and analyses data from different sensor technologies, such as Micro-Electro-Mechanical-System (MEMS) accelerometers, fibre optic (FO) sensors (e.g., Fiber Bragg Grating, FBG, and distributed backscattering based), and a weather station, described in the following sections.

3.1. Accelerometers (MEMS)

Triaxial MEMS accelerometers located at various locations within the industrial plant are connected to the dynamic acquisition system (dDas) to monitor for excessive ground accelerations (i.e. initiation of earthquakes) and to periodically store environmental vibration data useful for the identification of structural dynamic parameters [11]. The dDas consists of a standalone acquisition board capable of acquiring, filtering and processing up to 32 simultaneous analogue channels with 24bit precision analogue to digital converters. This module features sample rates of up to 1 kHz for dynamic acquisitions or periods from 1sec to 24hrs for static acquisitions. The signals recorded via these accelerometers are used as inputs for the structural RIE module, as shown in Fig. 1.

3.2. Fibre optic sensors

In recent years, the use of fibre optic (FO) sensor technologies in engineering and industrial applications has been increasing [12–15]. This is primarily attributed to the several advantages they hold with respect to traditional sensors, such as being lightweight and durable, possessing immunity to electromagnetic fields, high sensitivity, good embeddability, and the capability of covering wide areas. For example, FO sensors have been widely applied in down-well temperature measurements, structural monitoring of oil rigs, and detection and security monitoring of potential pipeline leakages. Given the notable possibilities of the FO sensors [16,17], both Fiber Bragg Grating (FBG) and Brillouin backscattering distributed sensors [18,19] are used in the ROSSINI platform to collect and provide the emission data necessary for the environmental RIE module (Fig. 1). FBG sensors are point sensors available for a wide range of measurements that can be used to build a large sensor network and be repeatedly queried at high frequencies. Brillouin distributed systems exploit the full length of an optical fibre as a strain and temperature sensor and, consequently, they are quite suitable for pipeline monitoring.

Because of depressurisation along with temperature drops following gas leakages from pressurised vessels or pipes, both pressure and temperature are monitored to detect possible gas releases into the local environment. For this purpose, FBG sensors can be used to measure localised pressure and temperature variations at specific locations of the test vessel as part of the ROSSINI project. Distributed Brillouin sensors may be employed to measure temperature variations on a wide area of the surface of the same test vessel. Both

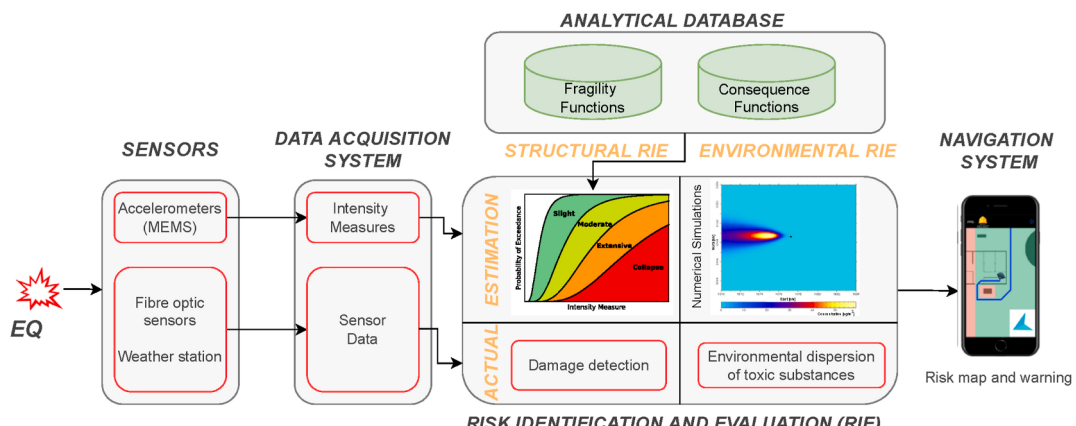


Fig. 1. Flowchart of the ROSSINI project.

types of sensors are connected to specific interrogation units through standard optical cables and connectors. The interrogation units are then connected to the ROSSINI server, capable of gathering data locally and sharing information throughout the online platform developed within the ROSSINI project shown in Fig. 2.

3.3. Weather station

The environmental RIE shown in Fig. 1 requires additional input data, which is to be provided via a weather station equipped with a wind speed sensor, a thermogravimetric sensor, in addition to a wind direction and a solar radiation sensor used to estimate the atmosphere stability, as depicted in Fig. 3.

3.4. Data acquisition system

As illustrated in Fig. 4, the data acquisition system consists of multiple sensors installed in the local environment, distributed processing units (data acquisition board), and data integration and filtering module running on the ROSSINI server, where robustness and redundancy are of prime importance in the design phase.

In the field of data acquisition, the novelty of the ROSSINI system lies in the possibility of exploiting different sensor technologies (i.e., MEMS accelerometers, FO sensors, and weather stations) depending on the specific plant's needs and strategies agreed with the plant ownership. The hardware architecture is designed to be robust and redundant to problems that can occur during earthquakes or serious damages to facilities which can compromise the safety and functionality of the monitoring and alerting system. To ensure the proper functionality in case of failure of the electrical system, the acquisition board is also equipped with a battery that guarantees 12 h of service and a solar panel to recharge it during the sunlit hours of the day. Additionally, the board electronics are suitably protected from accidental shocks or falling rubble by a rigid plastic box, allowing the system to operate in adverse conditions and harsh environments. Finally, the acquisition board supports wired gigabit connection to the local area network and wireless 4G/LTE modem. The physical connection is the most reliable and efficient one currently available and it is used as principal connection, whereas the wireless one is used as a fail-safe option. Although secondary, the wireless connection allows for sharing real-time data to the ROSSINI server with minimum latency.

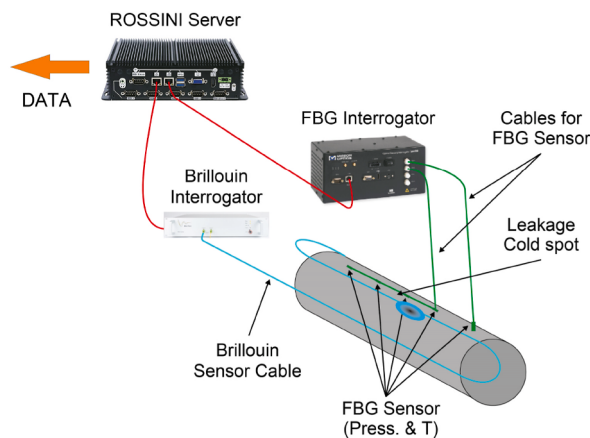


Fig. 2. Schematic of the proposed FO system.

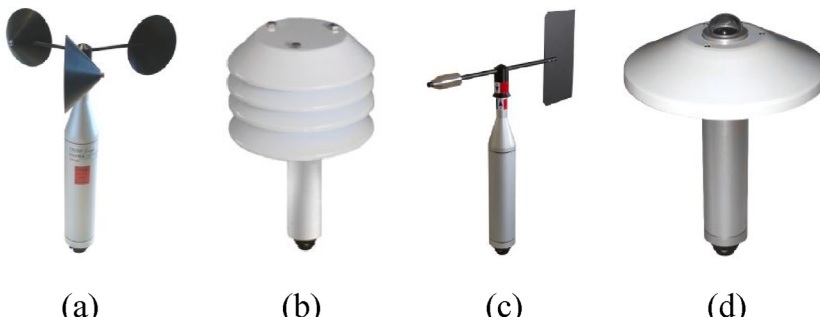


Fig. 3. Weather station comprising of (a) wind speed sensor; (b) thermogravimetric sensor; (c) wind direction sensor; and (d) solar radiation sensor.

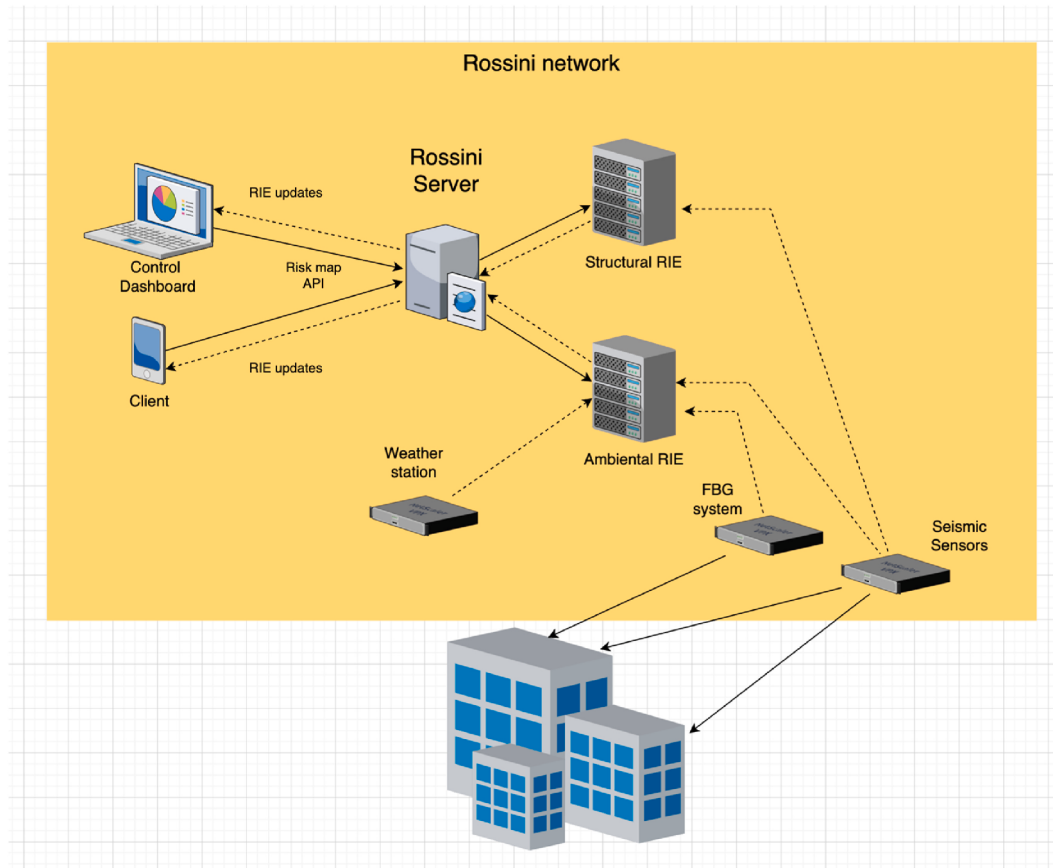


Fig. 4. Illustration of sensors and their interaction within the RIE modules.

4. Construction of the database

Vulnerabilities and consequences of all components and buildings within the plant area are identified for risk estimation. All components identified have fragility functions based on an intensity measure (IM) of either peak ground acceleration (PGA) or spectral acceleration at a first mode period and with specified damping, $Sa(T_1, \xi\%)$. Since only the potential life safety risk of collapsing structural or non-structural components is necessary for the risk-aware navigation of plant workers, only the damage states (DSs) having potential harmful consequences in this context are considered.

Fragility functions may be developed using either computational methods or experimental studies. For example [20], employed incremental dynamic analysis (IDA) to derive fragility curves for the buckling limit state of anchored steel tanks [21]; derived fragility curves of 3D RC pipe racks using IDA accounting for soil-structure interaction effects [22]; utilised a regression-based approach to derive fragilities for steel tanks with various levels of oil filling and water storage [23]; derived fragility functions based on seismic performance of over 400 tanks in 9 earthquake events, among others [24,25]. [26] derived fragility curves of piping systems for different grooved fit joints based on experimental results [27]; developed fragility functions of fire sprinkler piping systems based on the results of experimental testing, while [28] derived fragility parameters of fire sprinkler piping systems using a combination of shaking table experiments and numerical models. The approach adopted for ROSSINI herein employs both numerical analysis and available literature to construct the database of components with relevant fragility functions. Numerical models of precast concrete structures, ductile and non-ductile moment-resisting frame (MRF) structures were created to analyse various building typologies considered and the relevant DSs utilised within the scope of this project were identified.

Additionally, the behaviour of large liquid storage tanks during earthquakes has an importance far beyond the economic value of tanks and contents. For example, following the 1964 Niigata earthquake in Japan and the 1964 Alaska earthquake, the failure of tanks storing combustible materials, such as gasoline and other petroleum products, led to extensive, uncontrolled fires (Fig. 5). Throughout the years, extensive damage has been found for steel tanks that were not properly designed or detailed against seismic action [29–32], with the most common types of damage and failures including the buckling of the tank shell, roof damage due to convective wave motion, settlement of foundations, failure of piping systems connected to the tanks, plastification of the base plate in unanchored tanks due to uplifting, sliding of the tank, failure of anchor bolts and spillage of toxic material due to excessive sloshing [31,33]. To account for this, three different tank configurations with different aspect ratios were considered, each having broad (Tk-1), intermediate (Tk-2), and slender (Tk-3) structural configurations with different filling levels of 90% and 80% of their total capac-



Fig. 5. Steel tanks on fire during the 1964 Alaska earthquake (<https://www.valdemuseum.org>) (left), steel tanks on fire during the 1964 Niigata earthquake [1] (right).

ity, given its impact on the dynamic response of the structure. For example, an intermediate tank with 90% filling is generally less susceptible to damage due to the yielding of the structural shell when compared to the elephant foot buckling of the shell. In contrast, there is a significant increase in capacity of a latter with respect to the former with reduction of liquid height. Given the increase in capacity with the reduction of liquid filling, for the sake of simplicity, tanks with high liquid storage fillings were considered within the scope of the study. Additionally, broad tanks have considerably lower capacity when compared with slender tanks. The tanks were assumed to be anchored to the ground through Grade 8.8, M39 anchor bolts. Tank 1 was unanchored while tanks 2 and 3 were assumed to contain gasoline and a shell material of steel (S235). The tanks were designed following Eurocode 8 Part 4 [34], while the non-linear dynamic analysis was carried out through OpenSees [35]. Given the steel shell of the liquid storage tanks, 2% damping was assumed [36,37].

Assuming hydrodynamic effects, the tanks were idealised by an equivalent spring-mass mechanical model originally developed by Ref. [38] for dams and reservoir systems, which was later modified into a simple two-degree-of-freedom mechanical model to simulate the tank-liquid system response by Ref. [39]. Extensive non-linear dynamic analyses using the incremental dynamic analysis (IDA) [40] method were carried out using the numerical models of buildings and liquid storage tanks. To this end, the INNOSEIS record set [41] representative of the European medium seismicity context is selected as an appropriate strong motion suite. The IDA results were then used to generate fragility functions characterising the interface between structural response and expected levels of ground shaking intensities considering a specific IM of choice. The fragility database was largely based on numerically generated fragility functions developed either within the scope of ROSSINI or from available literature, which requires further work with possible considerations of ageing and deterioration impacts on components' fragility function parameters [42]; however, for ROSSINI the derived and utilised fragility database is deemed sufficient given the scope of the project. The fragility functions are assumed to follow a cumulative lognormal distribution and their parameters developed within the scope of ROSSINI are provided in Table 1 and Table 2. Similarly, the fragility functions associated with the process equipment and pipelines were adapted from available literature

Table 1
Derived fragility function parameters of the components considered.

ID	Component	Source	DS	Consequence	IM	Median [g]	Dispersion
PC-1-3ST	Multi-storey (3 storeys) precast concrete structure	Numerical modelling	Collapse DS	Complete collapse of structural system	PGA	1.19	0.42
PC-2-5ST	Multi-storey (5 storeys) precast concrete structure				PGA	1.25	0.30
D-BF-RC-4ST	Ductile bare MRF structure				PGA	1.69	0.42
ND-IF-RC-2ST	Non-ductile infilled MRF structure				PGA	1.31	0.34
Tk-1-90	Broad liquid storage tank with 90% filling level (unanchored)		Elephant foot buckling of shell	Damage to structural shell	$Sa(0.23, 2\%)$	1.82	0.37
Tk-2-80	Intermediate liquid storage tank with 80% filling level (anchored)				$Sa(0.14, 2\%)$	2.52	0.17
Tk-2-90	Intermediate liquid storage tank with 90% filling level (anchored)		Yielding of structural shell	Panel joint failure as a result of excessive deformities in the structural shell	$Sa(0.16, 2\%)$	1.80	0.13
Tk-3-90	Slender liquid storage tank with 90% filling level (anchored)				$Sa(0.15, 2\%)$	2.97	0.14

Table 2

Fragility function parameters of process equipment and pipelines adopted from literature.

ID	Component	Source	DS	Consequence	IM, [g]	Median	Dispersion
PR-SI	Pipe racks with soil-structure interactions considered	Di Sarno and Karagiannakis [21]	CLS	Complete failure, risk to human life, release of hazardous material	PGA	0.45	0.15
HZ1	Electrical equipment	HAZUS, MH 2.1 [24]	DS3	Failure of 40% of disconnect switches, or circuit breakers, or current transformers		0.50	0.60
HZ2	Boilers and pressure vessels	HAZUS, MH 2.1 [24]	DS3	Considerable damage		0.52	0.70
HZ4	Motor driven pumps	HAZUS, MH 2.1 [24]	DS4	Considerable damage		1.28	0.34
HZ7	Boiler building	HAZUS, MH 2.1 [24]	DS5	Complete DS of building		1.50	0.80
F1	Transformers, D5011.011d	FEMA P58-3 [43]	Inoperative	N/A		1.01	0.60
F2	Generator, D5092.031c	FEMA P58-3 [43]	Inoperative	N/A		0.90	0.40
E1-T	Ammonia storage vessel	PEC [25]	PL2	Complete release of content and global collapse of the vessel		0.54	0.46
E8-T	Compressor intercooler	PEC [25]	PL2			0.54	0.46
E13-T	Waste heat boiler	PEC [25]	PL2			0.54	0.46
E10	Reactor	PEC [25]	PL2	Global collapse of the vessel and the consequent release of fluid content		0.51	0.45
E7	1st stage air compressor	HAZUS, MH 2.1 [24]	DS4	Building or pumps badly damaged beyond repair		0.77	0.65
E9	2nd stage air compressor	HAZUS, MH 2.1 [24]	DS4			0.77	0.65
E21	Nitric acid unanchored tank (60%)	HAZUS, MH 2.1 [24]	DS4	Tank damaged and out of service		0.68	0.75
E28	Vertical water pump	HAZUS, MH 2.1 [24]	DS4	Considerable damage		1.25	0.60

*PL2 – complete release of content and global collapse of vessel, DS3 – moderate damage, DS4 – extensive damage, DS5 – complete damage, CLS – collapse limit state.

[21,24,25,43] and are given in Table 2. Since risk-aware navigation aims to ensure the life safety of plant workers, the performance limit states associated with slight or moderate damage are not of direct interest, but rather the collapse limit state which has the potential to cause harm. The estimated level of risk based on the fragility functions and associated input IM attained via the multi-sensor array will allow for the assignment of risk levels to be utilised within the risk-aware navigation system.

Additionally, an influence area based on component type and location was devised as a vulnerable zone, where possible debris falling can cause harm to workers. In case of damage, a risk value is assigned to the influence zone feeding toward the navigation system. Based on the available literature, the debris of collapsing reinforced concrete buildings with MRFs is assumed 85% of the total height of the building [44]. Based on engineering judgement and in lieu of available literature, the immediate risk area of equipment and non-structural components, such as liquid storage tanks, was taken as 50% of the total height of the component, and the influence zone was taken as 100% of the total height. Finally, the assumed value of influence area is not meant to be referential but rather a layered demonstration of the complex nature of the navigation system to consider various consequences. Further refinement based on more accurate data and observation can be easily utilised.

5. Risk identification and evaluation (RIE)

5.1. Structural RIE

The structural RIE module computes risk based on the probability of exceedance of specific DSs with adverse consequences to industrial workers. This is for both the structural and non-structural components and is computed for a given IM attained via the array of sensor technologies installed throughout the industrial plant. This is instead of using empirical data to define the fatality model factors presented in the literature, as the specific risk at any given location and time is necessary to ensure the safety of a single person. The use of fragility functions allows the direct estimation of the likelihood of components failing and accounts for the various uncertainties inherently present (e.g., ground motion record variability, modelling uncertainty); hence, these probabilities are used to indicate the possible impacts on passable terrain industrial workers may use as part of their egress in stable non-emergency conditions within the industrial plant area. Additionally, the values within empirical fatality models related to persons trapped under debris are irrelevant for the navigation purpose, as the trapped worker will be unable to escape, and alternative safety objectives and methods should be employed beyond the scope of this study.

Fig. 7 illustrates the risk estimation methodology utilised for the structural and non-structural components. Ten risk levels are assumed from 0 (no risk) to 9 (highest probability of risk of death) for the immediate zone, and 0 to 6 for the influence zone. Grouping them into bands of three, the risk levels from 1 to 3 describe low to high probability of minor injury, which are not considered within the navigation system due to no distinguishable aspect with respect to risk 0. Risks from 4 to 9 are associated with risk of injury requiring hospitalization all the way up, with increasing probability, to the risk of death. These risk levels were assumed at discrete thresholds of probability, the definitions of which should be studied further in future work. The collapse fragility function of vulnerable components is assumed to follow a typical lognormal distribution function given in Equation (1).

$$P[ds = DS|im] = \Phi\left(\frac{\ln im - \eta_{DS}}{\beta_{DS}}\right) \quad (1)$$

where η_{DS} is the mean value and β_{DS} is the logarithmic standard deviation for a given DS, P is the risk or probability of the actual ds being exceeded for a given im value, which is obtained from accelerometer multi-sensor array installed at various locations within the industrial plant. Integrating each component's collapse fragility function provided in [Tables 1 and 2](#) for a given level of seismic shaking, a real-time estimate of the probability can be estimated within the structural RIE. In [Fig. 7](#), for a given im , the probability of collapse is around 62%, which results in a structural risk level of 7 and 4 for the inside and the outside (influence zone) of the building, respectively. A similar approach is devised for non-structural components, where, instead of using the inside of a liquid storage tank, which is non-traversable by a worker, the immediate vicinity is considered based on engineering judgement, and the influence zone is derived further away from the immediate vicinity ([Fig. 6](#)).

5.2. Environmental RIE

Environmental health risk values describing the contamination levels in the local environment are mapped for identifying hot spot areas with higher risks for the workers' health. Health risks are calculated starting from the spatially resolved concentration field obtained by the atmospheric dispersion and compared against a set of chemical-specific toxicological thresholds to finally derive the severity level of the impacts on human health. An example of these is listed in [Table 3](#) for the case of benzene, but it is noted that the threshold values as well as the clinical manifestations will differ depending on the chemical substance. This environmental risk level is then combined with the structural risks computed in [Section 5.1](#), to get a unified risk map, discussed in the next section, which provides guidance to minimise the overall health risk for workers. The goal of this section is to estimate the second part of the combined risk metric (environmental health) and provide it as input to the navigation system, which then calculates the safest exit path from the industrial plant ([Section 6](#)).

5.2.1. Calculation of environmental dispersion of released toxic substances

Atmospheric dispersion models are generally used to simulate the accidental continuous, transient, instantaneous, or catastrophic release of chemicals from industrial plants, to predict concentration levels of toxic substances in the surrounding environment. Following recommendations by the Environmental Protection Agency [[45](#)], the Gaussian plume model ISCST3 has been selected among different dispersion models, also considering its fast execution time needed for real-time application, which is the case for the risk-based navigation system developed here. It has to be pointed out that the selected model has some limitations which include, for example, the inability to treat calm wind situation (i.e., wind speed $< 0.1 \text{ m/s}$), or the chemical transformations that may undertake the primary substance emitted or the fact that the turbulence processes within the atmospheric boundary layer are not taken duly into consideration. These limitations might be overcome by more sophisticated air quality models such as the photochemical Eulerian

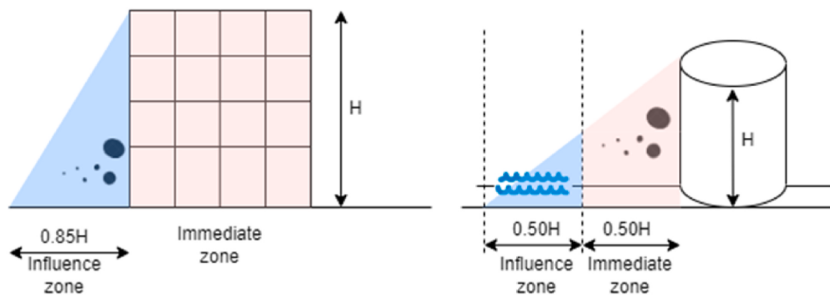


Fig. 6. Definition of influence zones for (left) structural and (right) non-structural components.

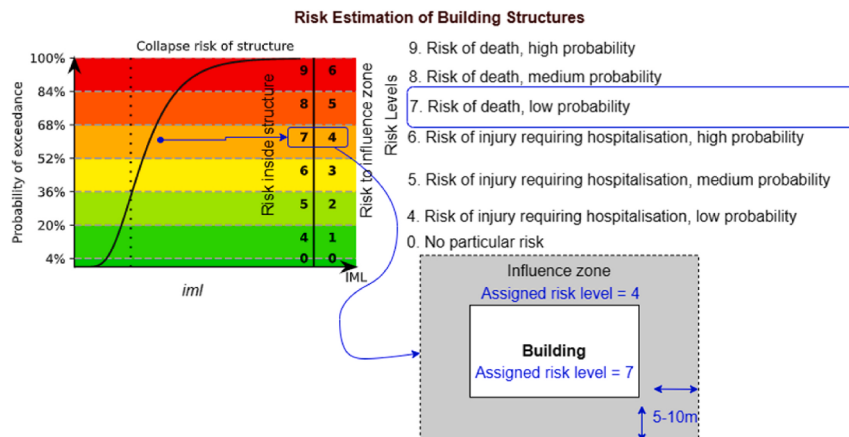


Fig. 7. Estimation of structural risk metrics inside and outside (influence zone) of a hypothetical building.

Table 3

Clinical manifestations severity based on benzene risks thresholds.

Level	Concentration (ppm)	Clinical manifestations	Tier level	Level of disability (Tier and emergency intervention)
0	0.1–5	No medical problems	0	–
1	5–10	No medical problems	0	–
2	10–25	Mild skin and ocular irritation	1	(1): Can be managed at the pre-hospital level
3	25–52	Transient systemic alterations, primarily nausea, mild drowsiness and headache	1	(1): Can be managed at the pre-hospital level
4	52–100	Drowsiness, dizziness, headache, initial mental status alterations (e.g., euphoria), pronounced mucous membrane, skin, eye, nose, pulmonary irritation	2	(2): Require admission to hospital
5	100–300	Pronounced drowsiness preceded by excitatory symptoms, staggering, weakness, impaired ability to take protective action	2	(2): Require admission to hospital
6	300–800	Excitatory symptoms followed drowsiness, staggering, impaired ability to take protective action, palpitations, tightness of the chest, blurring vision	3	(3): Require prompt hospitalization and intensive care support especially in subjects presenting neurological and cardiac alterations
7	800–1000	CNS depression, loss of consciousness, arrhythmias, shallow and rapid respiration, signs of pneumonitis, lethality in the most susceptible individuals	4	(4): Require on site stabilization and resuscitation measures
8	1000–4000	Severe CNS depression, coma, paralysis, convulsions, non-cardiogenic pulmonary edema, lethality	4	(4): Require on site stabilization and resuscitation measures
9	>4000	As above, rapid deterioration and loss of physiological function, lethality	4	(4): Require on site stabilization and resuscitation measures

models which, on the other hand, need a huge number of input parameters not always available and long computational time that does not fit the need of a real-time application.

In the ISCST3 model, concentration inside the plume is predicted by Gaussian statistics, with the centreline of the plume at the maximum of the Gaussian distribution and with the standard deviation of the Gaussian distribution increasing as a function of time or downtime distance. The ISCST3 model allows the three-dimensional concentration field to be described during the release of material, produced by a point source under steady-state emission and meteorological conditions [46] (Equation (2)).

$$c(x, y, z) = \frac{Q}{2\pi\sigma_y\sigma_z u} \exp\left(\frac{-y^2}{2\sigma_y^2}\right) \left(\exp\left(\frac{-(z-h)^2}{2\sigma_z^2}\right) + \exp\left(\frac{-(z+h)^2}{2\sigma_z^2}\right) \right) \quad (2)$$

where c is the pollutant concentration at a given location, Q is the source term, x is the downwind speed, y is the crosswind speed, z is the vertical direction and u is the wind speed at the height of the release h . The $\sigma_y = I_y x$ and $\sigma_z = I_z x$ deviations describe the cross-wind and vertical mixing of the pollutant, where I_y and I_z are the turbulent wind speed fluctuations in the y and z directions, respectively. Values of dispersions are determined by the magnitude of the turbulence in the atmosphere based on the Pasquill method [47]. Fig. 8 illustrates the spreading pattern of pollutants from a point source. The concentration of pollution downwind from a source is treated as spreading outward from the centreline of the plume following a Gaussian distribution. The plume spreads both horizontally (y -direction) and vertically (z -direction).

5.2.2. Quantitative calculation of toxic releases based on data from sensors

The Gaussian plume model ISCST3, used for modelling the environmental dispersion of toxic substances, requires data on both emission (i.e., chemical name, release rate, the equivalent diameter of the leak area, height above the ground level of the release, geo-

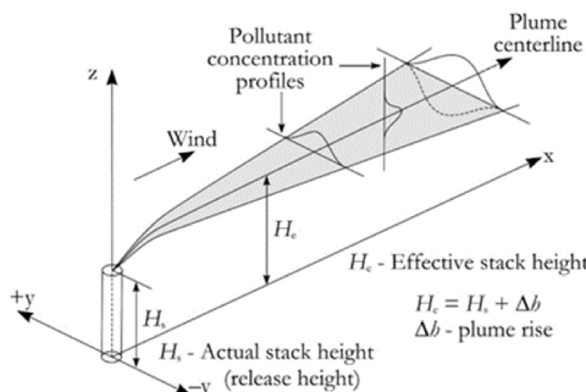


Fig. 8. Diffusion of pollutants from a point source [48].

graphical coordinates of the release point, temperature, physical state and exit velocity of the emitted substance) and meteorological (i.e., wind speed and direction, air temperature, atmospheric stability, Pasquill class and height of atmospheric mixing layer) as its input. Measurements from both FBG and distributed backscattering-based sensors can be exploited for assessing emission data (Section 3.2), while a meteorological station provides the necessary meteorological data (Section 3.3). To quantitatively compute the release of toxic substances based on data from sensors, a simplified analytical model for the analysis of the discharge process of a pressurised vessel has been developed. The proposed model allows the estimation of the average outflow rate and leak area based on pressure and temperature measurements acquired from FO sensors. The simplified model assumes a thermally and calorically perfect gas in the vessel. The average velocity of the fluid in the tank is considered negligible compared to the leakage velocity, and the contribution from gravitational potential energy is neglected. The leakage hole is modelled as a converging nozzle, with isentropic and quasi-unidimensional flow [49,50]. By modelling the opening of a leak as a converging nozzle, the instant mass outflow rate (\dot{m}_{out}) can be quantified depending on sonic (Equation (3)) or subsonic conditions (Equation (4)).

$$\dot{m}_{out} = \begin{cases} A_l P \sqrt{\frac{kM}{RT}} \cdot \sqrt{\left(\frac{2}{k+1}\right)^{\frac{k+1}{k-1}}} & (3) \\ A_l P \sqrt{\left(\frac{2k}{k-1}\right) \frac{M}{RT} \left(\frac{P_B}{P}\right)^{\frac{2}{k}}} \left[1 - \left(\frac{P_B}{P}\right)^{\frac{k-1}{k}}\right] & (4) \end{cases}$$

where A_l is the leak area; P and T are the pressure and the temperature of the gas in the vessel; P_B is the ambient pressure; k is the gas-specific heat ratio; M is the molar mass and R is the gas constant. The simplified analytical model also allows the discharge time and total gas mass out of the vessel to be assessed, which are essential for estimating the average outflow rate and in line with input data required by the Gaussian models. Sensor data from optical fibres are then coupled with meteorological measurements and numerical simulations for estimating concentrations of chemicals in the industrial plant and simulating their spatial diffusion over time, as required by the environmental part of the RIE module.

5.3. Combined risk

A combined risk metric is then computed based on the structural and environmental risks estimated in previous sections. In cases where two risk values are available from both structural and environmental RIEs, the maximum of the two is used to populate the map. This was a rather simple user choice made here to develop the system but more detailed consideration of the interaction of risks could be investigated in the future. For example, it was initially hypothesised to use an averaged value, but in cases where one risk was high (e.g., 9) and the other was low (e.g., 1), this would result in an artificially lower value (e.g., 5) that could indirectly lead user through an area with a high risk and expose them to harm. This combined map is then fed into the navigation system and communicated to the industrial plant worker's mobile device. It is important to underline that structural and environmental health risk levels are not necessarily driven by the same causative factors, meaning that depending on the IM level of the recorded ground motion, the structural risk might be estimated as level 3, while due to the concentration levels of toxic substances released, the environmental health risk might be estimated as level 7, or vice versa. This is because the structural RIE is tied to the type of the building or the non-structural component, its functionality and type of collapse mechanism, whereas the environmental RIE is associated with the probability of release of toxic substances. Based on the example provided and the combination rule employed within this study, the combined risk of level 7 (i.e., computed as the maximum of 3 and 7) is fed into the navigation system for that particular cell of the map. A limitation of this approach stems from independent consideration of risk associated with structural and environmental risks. However, given the possibility of including more risk metrics, as well as the exploration of different pertinent aspects towards the computation of risk values (e.g., air pollution, leakages, structural, non-structural collapse), Graph Theory could be utilised more effectively in future expansions of the study.

Additionally, it is unlikely that environmental health risks will be present within an administrative building but more likely throughout the industrial plant where high-pressure piping and vessels are located. Furthermore, the spatial distribution and relative placement of structural and non-structural components act as key parameters that form the navigable area for identifying safe paths for workers to take for an exit. Finally, it is also assumed that the industrial plant worker can move freely with impediments and not be trapped under debris.

6. Implementation of the navigation system

6.1. System architecture

With the risk across the industrial plant's layout estimated from the approaches defined previously, the ROSSINI system now proceeds with the navigation of the industrial plant workers. The system architecture is provided in Fig. 9 and its main components are:

- A mobile device running the client application that guides the worker during emergencies;
- The ROSSINI server, that acquires sensor data and uses it to compute the combined risk-map; the risk-map is then transmitted to the client;
- A set of sensors that communicate with the ROSSINI server either directly or through a data acquisition board.

The ROSSINI server includes various modules, in particular:

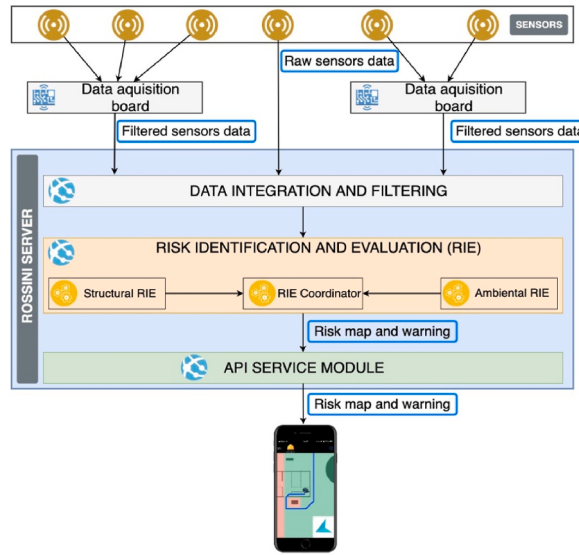


Fig. 9. ROSSINI system architecture.

- A data integration and filtering module, which receives raw data from the sensors, integrates and filters the data before providing them to the RIE modules;
- The RIE module, which integrates the structural and environmental RIEs (Section 5.1 and 5.2, respectively) combining the risk and creating the risk map;
- The API service module, which provides the risk-map to the mobile client, and raises a warning when a potentially dangerous situation occurs.

6.2. Mobile app

When creating the navigation app, two primary issues have emerged: 1) how to reliably compute the precise user location (including their position and orientation); and 2) how to interact with the user to effectively guide them along the safest route. After considering the state of the art, two solutions addressing these problems were devised for the purposes of this project:

- Positioning: a hybrid solution based on a combination of indoor and outdoor positioning techniques is used. The outdoor solution uses the operating system APIs (which combine GNSS, WiFi and cellular positioning), and the indoor solution uses an *ad-hoc* technique based on fiducial markers and visuo-inertial navigation (Fig. 10). This solution provides an advantage of avoiding the use of external radio signals (which might not be available in emergencies) and allows computation of the user's orientation, in addition to their location. Additionally, the solution relies on augmented reality, which is implemented in stable and well-maintained libraries.
- Navigation instructions: a solution was devised and depicted in Fig. 11, which is based on both allocentric and egocentric maps. When the user's location and orientation are known with high precision, the system shows navigation information using an

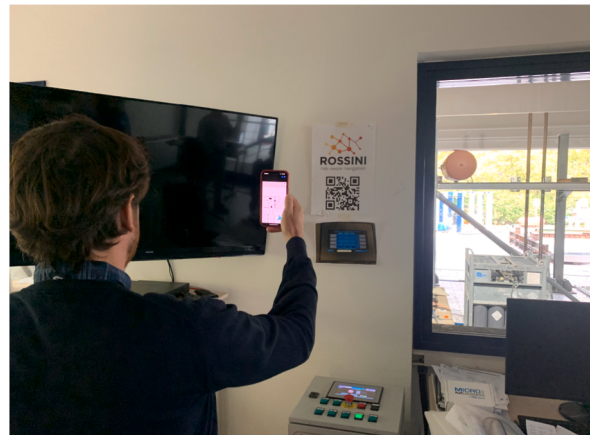


Fig. 10. Indoor positioning technique via ad-hoc solution based on fiducial markers and visuo-inertial navigation.

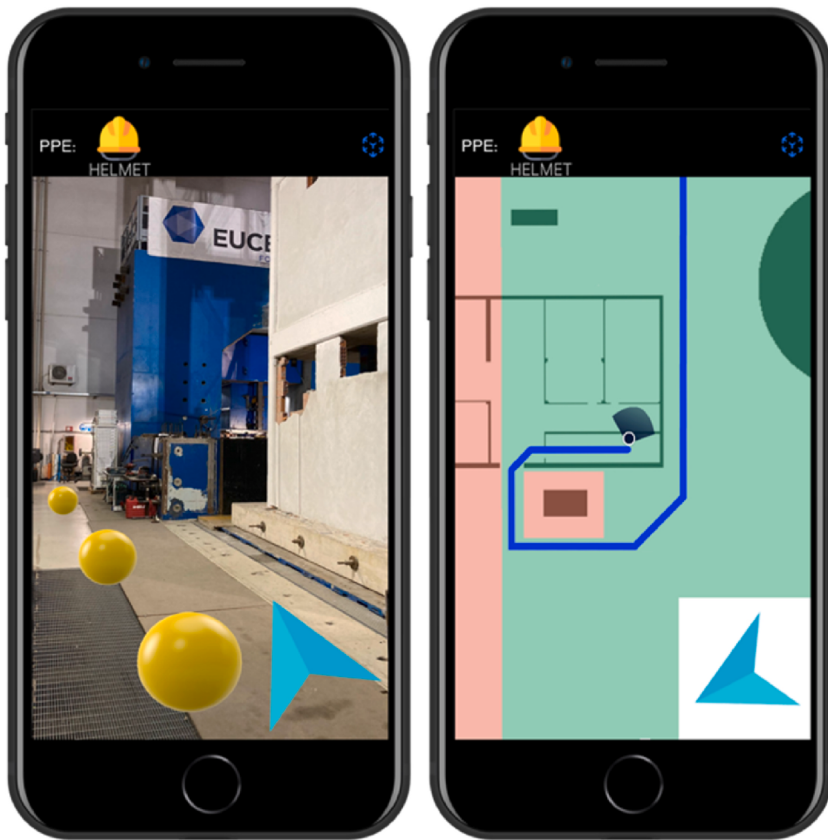


Fig. 11. ROSSINI mobile Client. Egocentric navigation (left); allocentric navigation (right).

egocentric map and an augmented reality to better guide the user (Fig. 11(left)). Otherwise, the system shows the map with an egocentric approach (Fig. 11(right)). In both cases, a multi-modal approach is adopted, combining visual information with audio and haptic information. In particular, the app adopts sonification techniques derived from the literature in the field of assistive technologies for people with visual impairments [51,52].

The risk-aware route is computed based on the client's starting position from two data structures: the *risk-map* and the *routes-graph*. The latter is a directed graph representing all the walkable paths. It models the area into discrete cells and considers the physical characteristics of the environment, like the walls and the emergency door (that can be traversed in one direction only). Starting from an area planimetry, an external app (i.e., not mobile) discretises the space into cells and creates a node for each cell as well as the connections between nodes (e.g., two adjacent nodes are connected if there is no wall between them). Fig. 12 shows an example of the discretised map, where black pixels represent walls, while the green arrows start from the centre of a cell and indicate which adjacent cells are connected. Red segments represent emergency doors that can be traversed in one direction only (Note: two colours are used, lighter and darker red, to represent the direction in which the door can be traversed; the difference is hard to perceive visually but this is irrelevant as this information is processed by a program, not by a human), while grey segments represent doors that can be traversed in both directions. This graph is then serialised as a file and transferred to the mobile device, where it is loaded when the app runs.

While running, the app receives a new risk map as soon as it is available on the server. Once a risk map is received, the mobile app updates the weight of nodes in the *routes-graph* (e.g., if an area in the *risk-map* has a high risk, the nodes in the *routes-graph* contained

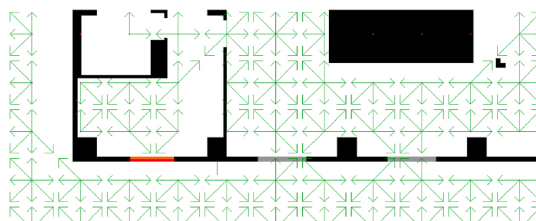


Fig. 12. Example of the area discretised into cells and their connections.

in that area are updated to have a high weight). Then, using an adaptation of the A* algorithm, the best route is computed from the current user's position to each safe area and the best route among them is selected. The "best route" is intended to mean the route that minimises the maximum risk value encountered, which is different to the typical implementation of A*, where the aim is to minimise the sum of the risk along the route. An example is shown in [Fig. 13](#). While the user is closer to the exit on the right-hand side of the map, the route to reach that exit would require to transit an area with risk level 9 (i.e., the purple colour that corresponds to tank). For this reason, the app suggests the route (i.e., the blue line) to the exit on the bottom-left, which is much further away but requires the worker to transit areas with maximum risk 3.

7. Case study application

7.1. Industrial plant layouts

For the demonstration of the risk-aware navigation system utilising integrated risks, a case study industrial plant layout was devised. Based on the review of past studies analysing the seismic risk of industrial plants [[53,54](#)], several representative industrial plant processes that can be considered typical for the scope of the ROSSINI project were identified. In these aforementioned studies, the conducted plant processes were typically described, and a subsystem of components was analysed. However, a complete spatial description of the entire plant's components and relative positioning was generally not available. The spatial description of the plant components and equipment with respect to one another was deemed a critical aspect necessary for the ROSSINI project. This is due to the navigation system requiring not only an individual measure of damage and potential risk of different parts of the plant but also their positioning, in addition to meteorological information to determine the likely patterns of potentially toxic material released into the local atmosphere.

To fill the missing gap, available plant layouts of several industrial facilities were made available to the ROSSINI project partners and analysed, where the relative distributions of the plant's components and buildings were deduced based on engineering judgement to provide a navigable area for a hypothetical worker. The case study plant consists of several buildings of various processes, multiple liquid storage tanks, storage vessels, piping arrangements as well as an electrical substation. The emergency exits have been hypothesised as external environments toward which the worker is navigated to avoid any risk of potential harm within the industrial plant. The plant layout allows a hypothetical scenario that could satisfy the needs of the ROSSINI project in terms of spatial distribution, damageable component details, positioning to identify meteorological and seismic parameters and overall scale. The scale of the industrial plant refers to the overall footprint area of the plant and the number of pertinent areas to be studied. The objective was not to overly complicate the case study and instead focus on a simple and clear illustration that could effectively illustrate the functionality of the ROSSINI system developed, with a view of future extension to other more complex and particular plant layouts.

With the above considerations in mind, two industrial plant layouts were devised. The first map, termed Map A ([Fig. 14](#)), was created for actual simulation purposes and testing of the navigation instructions communicated to the app for various scenarios. Specifically, two real buildings located in Pavia (Italy) were used as pseudo layouts for the industrial plant to simulate the application for terrain easily traversable in reality. This was deemed a fair compromise to test the functionality of the system and circumvented the need to obtain clearance access to actual industrial facilities several times over the course of the project's duration in order to test a navigation system. [Fig. 14](#) depicts the non-traversable terrain (i.e., structural, and non-structural elements) in black, while the terrain surrounding the buildings as well as within a traversable area of the buildings was used for analysis until the user reaches the safe zones (blue) in case of hazard. Emergency exits were used within the buildings for safe exits and have a one-way direction, from orange to red as previously noted. While Map A is based on a real terrain readily accessible for testing to the project consortium, it con-

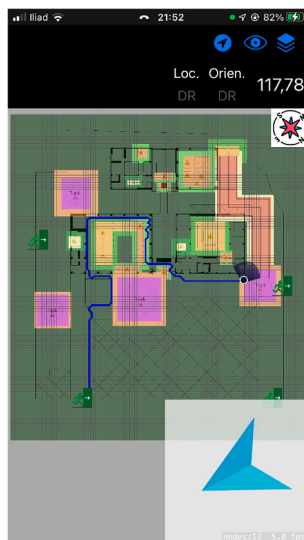


Fig. 13. Example illustration of how the navigation system takes the industrial plant worker along the safest path and not necessarily the closest.

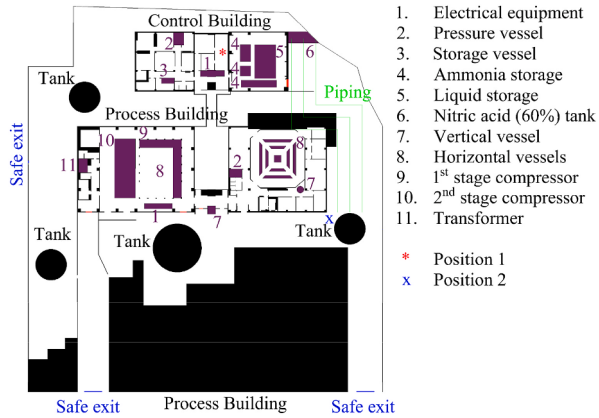


Fig. 14. Map A for on-site simulation purpose.

tains virtual components pertinent to industrial plants and aims to provide complex yet fictitious scenarios that can be navigated and extensively tested.

More in line with the layouts of actual industrial plants obtained during the project, the base map presented in Fig. 14 was enhanced to include various non-structural components such as tanks, piping racks, and storage vessels to simulate the effects of damaged components on the environment and workers' health in a virtual environment within a larger setting to form what is termed Map B, depicted in Fig. 15. In reality, Map A is an accessible subset of the much larger Map B. The advantage of having Map B is mainly for illustration and testing purposes with a larger set of damageable inventory and navigable area, to further demonstrate the navigation software's capabilities.

7.2. Testing scenarios

To demonstrate the practicality of the ROSSINI project presented in Fig. 1, it is crucial to do some functionality tests and confirm its capabilities against prototype case study industrial plant layouts presented in Figs. 14 and 15. Several scenarios were developed to demonstrate the RIE and navigation capabilities of the ROSSINI project. The scenarios varied in terms of map type, earthquake intensity, extent of release of the chosen substance, benzene, into the local atmosphere, and starting position of a worker within the map area. The ground motion recorded in L'Aquila, Italy, in 2009, with a PGA of 0.66 g, was selected from the NGA-West2 Database [55] and used as the reference seismic input triggering an emergency situation that industrial plant workers would need to navigate. As a result, five distinct scenarios were identified and are given in Table 4, where the different starting parameters are listed. All scenarios pertinent to Map A were tested on a local setting in person. This was done also through a series of in-situ experimental tests at the Eucentre Foundation's 9DLab shaking table (Fig. 16) and simulated environmental releases to test and verify the various sensors' (Section 3) functionality and implementability within such a system (Figs. 1 and 17). In contrast, the scenario pertinent to Map B was tested in a digital setting.

With regards the ground motion scaling factor, this comprised of a simple amplitude scaling of the input ground motion so that different levels of structural risk would result from the structural and non-structural components based on the fragility functions adopted. For the environmental parameters, a baseline scenario which reflected the worst-case scenario determined after comparing the results of several simulation tests was considered and comprised the following assumptions: (i) emission rate = 43.66 g/s; (ii)

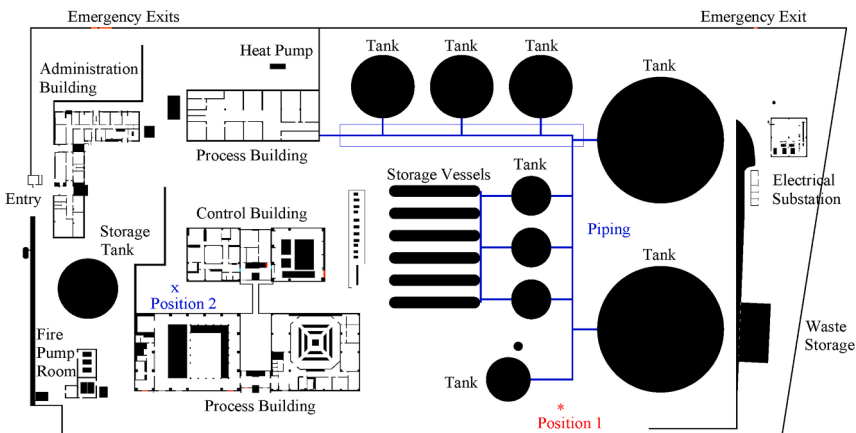


Fig. 15. Map B for simulation purposes in a virtual environment.

Table 4

Case study application scenarios.

Scenario	Map	Ground motion scaling factor	Environmental release scaling factor	Starting position
1	A	1.0	1.0	Position 1
2	A	0.0	1.0	Position 1
2a	A	0.0	0.03	Position 1
3	A	1.2	0.0	Position 1
3a	A	0.5	0.0	Position 1
4	A	1.0	1.0	Position 2
5	B	1.0	0.0	Position 2
6	B	0.8	1.0	Position 2
7	B	0.8	1.0 ^a	Position 1
8	B	0	1.0 ^a	Position 1

^a Two sources of environmental release.

Fig. 16. Shake table tests.

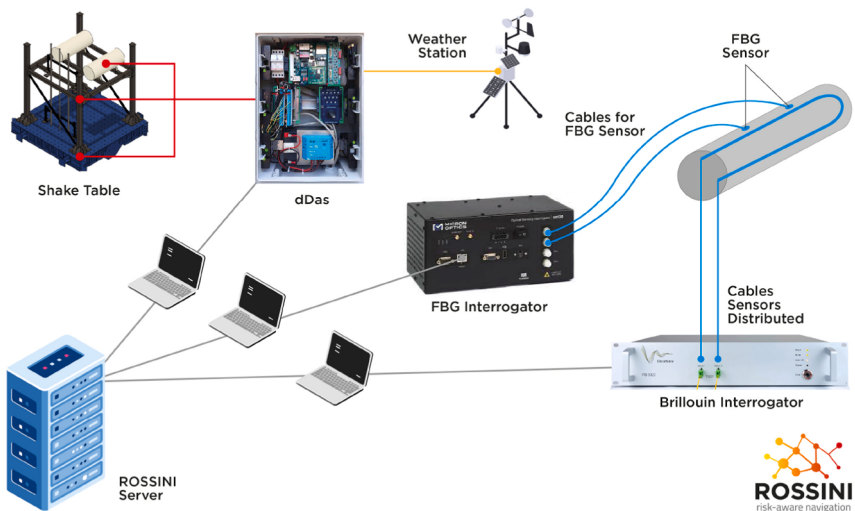


Fig. 17. Sensors' layout and connection to ROSSINI server.

height above the ground of the release = 1 m; (iii) temperature of the chemical released = 80 °C; (iv) exit velocity of the release = 10 m/s; (v) diameter equivalent of the rupture = 0.0019 m. In addition, to simulate a scenario with a lower environmental impact, an emission rate equal to 1.31 g/s was used, keeping all the other parameters reported above the same for the worst-case scenario. The ratio between this emission rate and the worst-case emission rate is then 0.03 as reported in Table 4.

The starting position of the user was also varied between scenarios so that different exit paths would result and illustrate the navigation system's ability to identify not the shortest path, but rather the lowest risk path, which was already discussed in Fig. 13.

Scenario 1 represents the baseline scenario with both structural and environmental RIE activation. In other words, the structural risk map was associated with the estimated and measured damage level, while the environmental risk map was associated with the measured release level of a toxic substance. The scenarios from 1 to 4 represent different variations via the scaling of the input ground motion and/or toxic substance release, as well as starting position of the user. Scenarios 5 to 8 are the demonstration of the navigation using Map B with similar variations to Map A in addition to inclusion of two sources of environmental releases within the map area considered for scenarios 7 and 8.

Each scenario with the navigation path computed and communicated to the mobile app are presented in Fig. 18. The map visible to the user on the app is the integration of both structural and environmental RIE maps. Within the map, the risk levels with an index from 0 to 9 are shown. The user frames the closest markers, as shown in Fig. 10, and the app calculates the user's current position, which is shown on each map. Based on the current position, the navigation system devises the least dangerous path to follow to the nearest safe exit, quantified as the one with the lowest maximum risk.

As observed from Fig. 18(a), with both structural and environmental risks, the user is forced towards the furthest possible exit, as the higher risk associated with the pipelines on the west side as well as the blocked passageways because of risks associated with liquid storage tanks make the nearby exits less desirable. Additionally, the building near the north side exit is at high risk of collapse, therefore the exit is not deemed a desirable target for the navigation system. Fig. 18(b) and (c) present Scenarios 2 and 2a, where the environmental hazards due to the release of toxic substances are activated only with different concentration levels. Here, due to no earthquake excitation, the buildings and non-structural components are unaffected, therefore, the navigation system directs the user towards the nearest safe exit. This scenario could also be considered representative of a non-seismic event situation that would require navigation. That is, through the array of sensors installed throughout an industrial plant, the ROSSINI system is capable of detecting leakages and toxic releases caused by other external impacts, communicating their occurrence to the workers, and providing instructions on how one may navigate to safety.

Fig. 18(d) presents Scenario 3, which is a variation of Scenario 1, where no release of toxic substances is foreseen, and the level of ground motion is increased through a scaling factor of 1.2, as a result, the entire Map A is coloured with notable risk levels. However, since the approach of the navigation system is not the selection of the lowest cumulative risk, but rather the minimal risk pathway, it returns an updated pathway compared to Scenario 1. In this case, the user is forced to circumvent the tank in the middle of the map through its northeast side and re-enter the building. Finally, the user exits the building again at a nearby gate leading towards the same safe exit as in Scenario 1. In contrast to Scenario 3, Fig. 18(e) presents Scenario 3a, where the intensity of the ground motion is reduced with respect to Scenario 3, resulting in lower risks throughout the entire map, which eventually led the user towards the nearest exit on the northwest side of the map. Fig. 18(f) demonstrates Scenario 4, which is a variation of Scenario 1, as it uses the same risk but a different position of a user. Even though the user is nearby the northwest safe exit, the navigation app recognises very

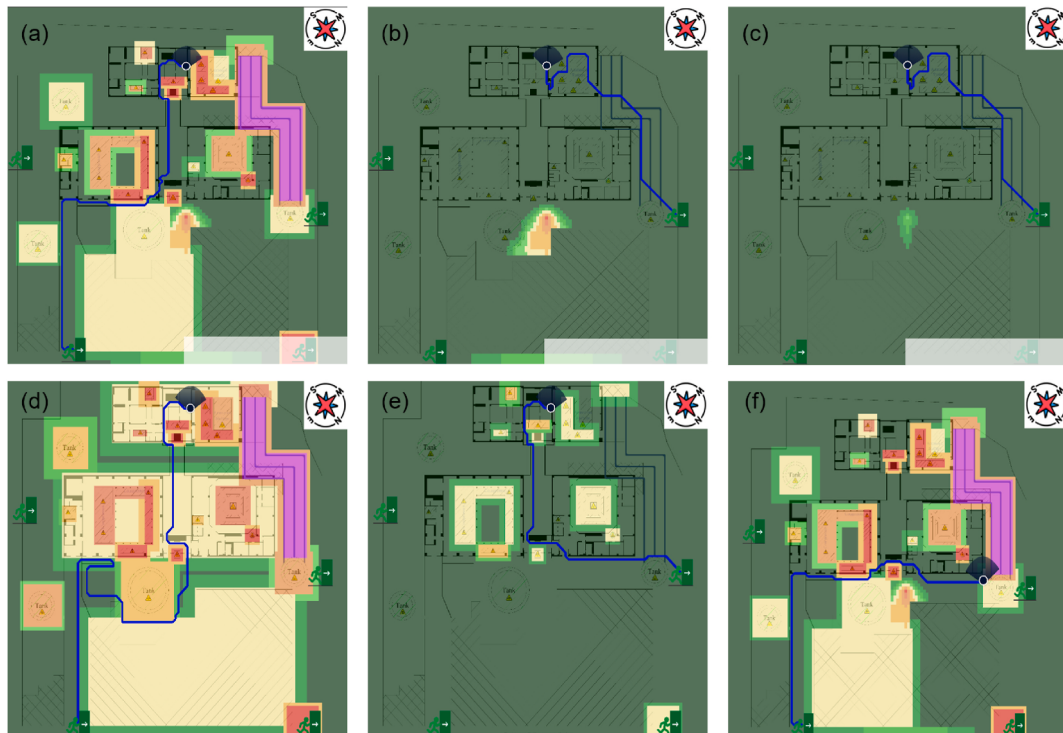


Fig. 18. Case study applications for Map A: (a) scenario 1; (b) scenario 2; (c) scenario 2a; (d) scenario 3; (e) scenario 3a; (f) scenario 4.

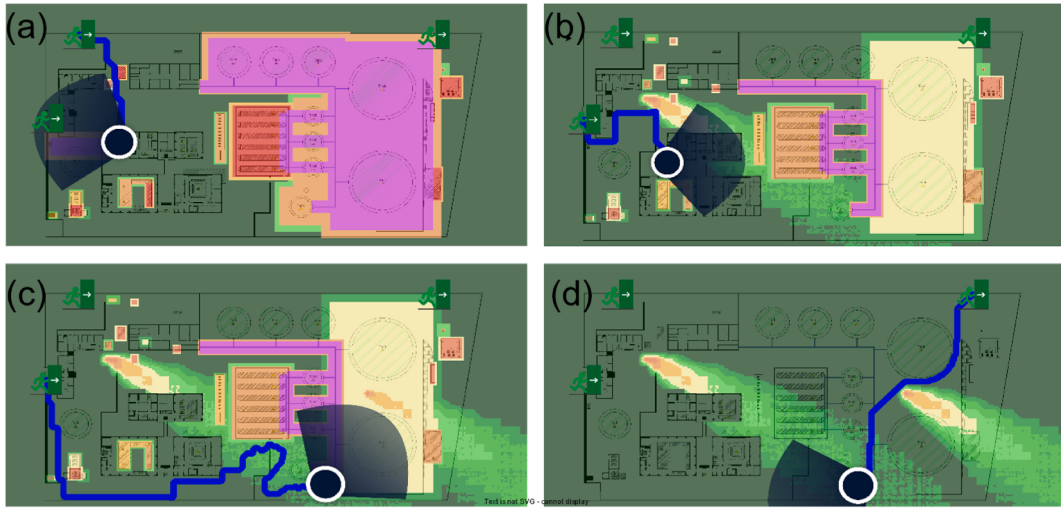


Fig. 19. Case study applications for Map B: (a) scenario 5; (b) scenario 6; (c) scenario 7; (d) scenario 8.

high risk due to nearby pipelines and tanks failing, which eventually results in a designated least-risk path towards the east exit, which was previously discussed in Section 6.

Fig. 19 presents the scenarios associated with Map B. Fig. 19(a) demonstrates Scenario 5, where only the structural risk is triggered. Here, the user is located in the proximity of two emergency exits, however, due to the vicinity of highly seismic zone near the emergency exit to the left of the map, the user is directed towards a slightly further exit at the top of the map. Scenario 6 varies with respect to Scenario 5, with the addition of environmental releases near the position of the user, and a reduced structural risk, as a result of which the user is directed towards the leftmost exit (Fig. 19(b)). To have further variations for the navigation, the user is assumed to be located near the highly congested area to the right bottom of the map. A second source of environmental release is introduced with the same characteristics. As a result of the new source of release as well as the position of the user, Scenario 7 (Fig. 19(c)) demonstrates a navigation path towards the leftmost exit through some areas with minor risk. In contrast, Fig. 19(d) includes only the environmental risks (Scenario 8) resulting in a shorter path towards the upper emergency exit as the tanks and piping systems are no longer dangerous for the safety of the user due to no earthquake shaking.

8. Summary and conclusions

An overview of the ROSSINI project's development was presented along with its implementation in the context of risk-aware navigation for industrial plant workers exposed to harm during seismic events. This implementation is enabled through various components of the system explained throughout the paper. The sensor technologies utilised were described in detail to demonstrate their integration as part of smart technologies to mitigate and manage risk following hazardous events. The component inventory database was compiled based on available literature and through a computational approach within the scope of ROSSINI. The structure risk identification and evaluation (RIE) module then estimates structural risk from the database of components posing a risk to workers. Similarly, the environmental RIE computes the risk by coupling sufficient theory on the diffusion of harmful substances with the sensor array that can detect leakages and other similar incidents. Finally, both structural and environmental risks are enveloped and the risks are mapped into a pre-selected plant layout for the navigation software to use. The architecture of the system was detailed through the introduction of two novel solutions to resolve potential issues associated with the location of a user within a plant area and the interaction with the user guiding them towards the exit via the safest route.

To demonstrate the capabilities of the ROSSINI project, the system was applied to two case study plant layouts. Multiple scenarios were employed, where the plant layout was varied, along with different scaling factors of ground motion records and environmental release, and a starting position of a user. The scenarios demonstrated the capability of the ROSSINI platform to generate the lowest-risk path for the users independent of whether one or both RIEs were activated and the level of activation. The navigation software as well as the combined risk computation techniques employed highlight an important step for increasing the safety of workers and managing the risk in industrial plants following hazardous events.

Overall, the ROSSINI project allowed the partners with notably different backgrounds to develop and implement their respective know-how in relation to: the combination of different sensor technologies on a single platform, the evaluation of seismic risk in an industrial plant context via a data-stream of combined risk estimates, the geolocation of risks within an industrial plant's layout and its communication to a navigation system built using different algorithms and libraries to arrive a final set of risk-based navigation instructions for the industrial plant workers.

The ROSSINI project served as a stepping stone to develop a prototype system capable of implementing each step of the process described here. Several aspects may be improved with further research and development. For example, the development of a more extensive and representative library of fragility and consequence functions to estimate structural risks with support of further through

experimental testing. Also, the utilisation of further sensor typologies that may be required in addition to those examined. The combination of risks was introduced here as a novel concept that could be further developed and refined. Regarding navigation, developing a means of initial user positioning that does not rely on specific markers could be explored along with where the computation of navigable paths is conducted (i.e., centralised server or local client) to handle situations where server-to-client connection cannot be guaranteed. Again, this is a prototype development with promising results and can be easily transferred and tested on real and larger industrial plants.

Declaration of competing interest

The authors declare that they have no known competing financial interests or personal relationships that could have appeared to influence the work reported in this paper.

Data availability

Data will be made available on request.

Acknowledgements

This work received financial support from the ROSSINI project funded by INAIL (Italian national institute for workplace insurance) under the call "BRIC 2019". The authors would like to acknowledge the contributions of Volkan Ozsarac and Al Mouayed Bellah Nafeh during the development of the component database presented in this study, Denis Sarigiannis for his input on the development of the environmental risk identification and evaluation approach and Giorgio Nosenzo and Massimo Facchini for their support in developing the FO system.

References

- [1] K. Suzuki, Earthquake damage to industrial facilities and development of seismic and vibration control technology, *J. Syst. Des. Dyn.* 2 (1) (2008) 2–11, <https://doi.org/10.1299/jsdd.2.2>.
- [2] M. Erdik, E. Durukal, Damage to and vulnerability of industry in the 1999 kocaeli, Turkey, earthquake, *Build. Safer Cities Futur. Disaster Risk* 8 (RMS 1999) (2003) 289–291.
- [3] S. Grimaz, Can earthquakes trigger serious industrial accidents in Italy? Some considerations following the experiences of 2009 L'Aquila (Italy) and 2012 Emilia (Italy) earthquakes, *Boll. di Geofis. Teor. ed Appl.* 55 (1) (2014) 227–237, <https://doi.org/10.4430/bgta0116>.
- [4] S. Esposito, S. Giovinazzi, L. Elefante, I. Iervolino, Performance of the L'Aquila (central Italy) gas distribution network in the 2009 Mw 6.3 earthquake, *Bull. Earthq. Eng.* 11 (6) (2013) 2447–2466, <https://doi.org/10.1007/s10518-013-9478-8>.
- [5] C. Christopoulos, A. Filiatrault, *Principles of Passive Supplemental Damping and Seismic Isolation*, IUSSpress, Pavia, Italy, 2006.
- [6] B.F. Spencer, S. Nagarajaiah, State of the art of structural control, *J. Struct. Eng.* 129 (7) (2003) 845–856, [https://doi.org/10.1061/\(ASCE\)0733-9445\(2003\)129:7\(845\)](https://doi.org/10.1061/(ASCE)0733-9445(2003)129:7(845)).
- [7] A. Coburn, R. Spence, *Earthquake Protection*, John Wiley & Sons, Inc, Chichester, UK, 2002.
- [8] H. Crowley, B. Polidoro, R. Pinho, J. van Elk, Framework for developing fragility and consequence models for local personal risk, *Earthq. Spectra* 33 (4) (2017) 1325–1345, <https://doi.org/10.1193/083116EQS140M>.
- [9] S.N. Jonkman, P.H.A.J.M. Van Gelder, J.K. Vrijling, An overview of quantitative risk measures for loss of life and economic damage, *J. Hazard Mater.* 99 (1) (2003) 1–30, [https://doi.org/10.1016/S0304-3894\(02\)00283-2](https://doi.org/10.1016/S0304-3894(02)00283-2).
- [10] A.R. Taig, F.E. Pickup, *Risk Assessment of Falling Hazards in Earthquakes in the Groningen Region*, 2016.
- [11] G.J. O'Reilly, D. Perrone, M. Fox, R. Monteiro, A. Filiatrault, I. Lanese, A. Pavese, System identification and seismic assessment modeling implications for Italian school buildings, *J. Perform. Constr. Facil.* 33 (1) (2019) 04018089, [https://doi.org/10.1061/\(ASCE\)CF.1943-5509.0001237](https://doi.org/10.1061/(ASCE)CF.1943-5509.0001237).
- [12] A. Barrius, J.R. Casas, S. Villalba, A review of distributed optical fiber sensors for civil engineering applications, *Sensors* 16 (5) (2016), <https://doi.org/10.3390/s16050748>.
- [13] H.N. Li, D.S. Li, G.B. Song, Recent applications of fiber optic sensors to health monitoring in civil engineering, *Eng. Struct.* 26 (11) (2004) 1647–1657, <https://doi.org/10.1016/j.engstruct.2004.05.018>.
- [14] A. Marino, M.M. Ciucci, in: C. Niezrecki, N.G. Meyendorf, K. Gath (Eds.), *Smart Approach to Integrated Natural Risks Management for Industry 4.0. " Smart Struct. NDE Energy Syst. Ind. 4.0."*, SPIE, 2019, p. 5.
- [15] F. Paolacci, G. Quinci, C. Nardin, V. Vezzari, A. Marino, M. Ciucci, Bolted flange joints equipped with FBG sensors in industrial piping systems subjected to seismic loads, *J. Loss Prev. Process. Ind.* 72 (March) (2021), 104576 <https://doi.org/10.1016/j.jlp.2021.104576>, Elsevier Ltd.
- [16] C.D. Butter, G.B. Hocker, Fiber optics strain gauge, *Appl. Opt.* (17) (1978) 2867–2869.
- [17] B. Glisic, D. Inaudi, Development of method for in-service crack detection based on distributed fiber optic sensors, *Struct. Health Monit.* 11 (2) (2012) 161–171, <https://doi.org/10.1177/1475921711414233>.
- [18] D. Garus, K. Kreber, F. Schliep, Torsten Gogolla, Distributed sensing technique based on Brillouin optical-fiber frequency-domain analysis, *Opt. Lett.* (21) (1996) 1402–1404.
- [19] M. Nikles, L. Thevenaz, P.A. Robert, Simple distributed fiber sensor based on Brillouin gain spectrum analysis, *Opt. Lett.* 10 (21) (1996) 758–760.
- [20] N. Buratti, M. Tavano, Dynamic buckling and seismic fragility of anchored steel tanks by the added mass method, *Earthq. Eng. Struct. Dynam.* (2014), <https://doi.org/10.1002/eqe.2326>.
- [21] L. Di Sarno, G. Karagiannakis, *On the Seismic Fragility of Pipe Rack—Piping Systems Considering Soil–Structure Interaction*, Bull. Earthq. Eng. Springer Netherlands, 2020.
- [22] I. Iervolino, G. Fabbrocino, G. Manfredi, Fragility of standard industrial structures by a response surface based method, *J. Earthq. Eng.* 8 (6) (2004) 927–945, <https://doi.org/10.1080/13632460409350515>.
- [23] M.J. O'Rourke, P. So, Seismic fragility curves for on-grade steel tanks, *Earthq. Spectra* 16 (4) (2000) 801–815, <https://doi.org/10.1193/1.1586140>.
- [24] FEMA, *HAZUS - MH 2.1 Technical Manual, Earthquake Model, Multi-Hazard Loss Estimation Methodology*, Federal Emergency Management Agency, Washington, D.C., 2003.
- [25] PEC, Deliverable D4.1 - definition of the structural models and seismic fragility analysis techniques available for the specific case study, PEC Project: Post-Emergency, Multi-Hazard Health Risk Assessment in Chemical Disasters, 2017.
- [26] T. Wang, Q. Shang, X. Chen, J. Li, Experiments and fragility analyses of piping systems connected by grooved fit joints with large deformability, *Front. Built Environ.* 5 (April) (2019) 1–14, <https://doi.org/10.3389/fbuil.2019.00049>.
- [27] Y. Tian, A. Filiatrault, G. Mosqueda, Experimental seismic fragility of pressurized fire suppression sprinkler piping joints, *Earthq. Spectra* 30 (4) (2014) 1733–1748, <https://doi.org/10.1193/111011EQS278M>.

- [28] S. Soroushian, A.E. Zaghi & E. "Manos" Maragakis, A. Echevarria, Seismic fragility study of displacement demand on fire sprinkler piping systems, *J. Earthq. Eng.* 18 (7) (2014) 1129–1150, <https://doi.org/10.1080/13632469.2014.917059>.
- [29] E. González, J. Almazán, J. Beltrán, R. Herrera, V. Sandoval, Performance of stainless steel winery tanks during the 02/27/2010 Maule Earthquake, *Eng. Struct.* 56 (2013) 1402–1418, <https://doi.org/10.1016/j.engstruct.2013.07.017>.
- [30] G.C. Manos, Evaluation of the earthquake performance of anchored wine tanks during the San Juan, Argentina, 1977 earthquakes, *Earthq. Eng. Struct. Dynam.* 20 (12) (1991) 1099–1114, <https://doi.org/10.1002/eqe.4290201202>.
- [31] A. Niwa, R.W. Clough, Buckling of cylindrical liquid-storage tanks under earthquake loading, *Earthq. Eng. Struct. Dynam.* (1982), <https://doi.org/10.1002/eqe.4290100108>.
- [32] F. Zareian, C. Sampere, V. Sandoval, D.L. McCormick, J. Moehle, R. Leon, Reconnaissance of the Chilean wine industry affected by the 2010 Chile offshore maule earthquake, *Earthq. Spectra* 28 (1_suppl1) (2012) 503–512, <https://doi.org/10.1193/1.4000048>.
- [33] E. Brunesi, R. Nascimbene, M. Pagani, D. Beilic, Seismic performance of storage steel tanks during the may 2012 Emilia, Italy, earthquakes, *J. Perform. Constr. Facil.* (2015), [https://doi.org/10.1061/\(asce\)cf.1943-5509.0000628](https://doi.org/10.1061/(asce)cf.1943-5509.0000628).
- [34] CEN, EN 1998-4 Eurocode 8 - Design of Structures for Earthquake Resistance - Part 4: Silos, Tanks and Pipelines, European Committee for Standardization (CEN), Brussels, Belgium, 2006.
- [35] F. McKenna, OpenSees: a framework for earthquake engineering simulation, *Comput. Sci. Eng.* (2011), <https://doi.org/10.1109/MCSE.2011.66>.
- [36] G.M. Calvi, R. Nascimbene, in: I. Press (Ed.), *Progettare I Gisci, Eucentre, Pavia*, 2011.
- [37] V. Ozsarac, E. Brunesi, R. Nascimbene, Earthquake-induced nonlinear sloshing response of above-ground steel tanks with damped or undamped floating roof, *Soil Dynam. Earthq. Eng.* 144 (2021) 106673, <https://doi.org/10.1016/j.soildyn.2021.106673>.
- [38] H.M. Westergaard, Water pressures on dams during earthquakes, *Trans. Am. Soc. Civ. Eng.* (1933), <https://doi.org/10.1061/taceat.0004496>.
- [39] G.W. Housner, The dynamic behavior of water tanks, *Bull. Seismol. Soc. Am.* 53 (2) (1963) 381–387, <https://doi.org/10.1785/BSSA0530020381>.
- [40] D. Vamvatsikos, C.A. Cornell, Incremental dynamic analysis, *Earthq. Eng. Struct. Dynam.* 31 (3) (2002) 491–514, <https://doi.org/10.1002/eqe.141>.
- [41] D. Vamvatsikos, C. Castiglioni, K. Bakalis, L. Calado, M. D'Aniello, H. Degee, B. Hoffmeister, M. Pinkawa, J.M. Proenca, A. Kanyilmaz, F. Morelli, A. Stratan, I. Vayas, A risk-consistent approach to determine behavior factors for innovative steel lateral load resisting systems, *ce/papers* 1 (2–3) (2017) 3434–3443, <https://doi.org/10.1002/cepa.398>.
- [42] J. Ghosh, J.E. Padgett, Aging considerations in the development of time-dependent seismic fragility curves, *J. Struct. Eng.* 136 (12) (2010) 1497–1511, [https://doi.org/10.1061/\(ASCE\)ST.1943-541X.0000260](https://doi.org/10.1061/(ASCE)ST.1943-541X.0000260).
- [43] FEMA, FEMA P58-3. Seismic Performance Assessment of Buildings Volume 3 - Performance Assessment Calculation Tool (PACT), 2012 (Washington, D.C.).
- [44] O.A. Sediek, S. El-Tawil, J. McCormick, Seismic debris field for collapsed RC moment resisting frame buildings, *J. Struct. Eng.* 147 (5) (2021) 04021045, [https://doi.org/10.1061/\(ASCE\)st.1943-541x.0002985](https://doi.org/10.1061/(ASCE)st.1943-541x.0002985).
- [45] EPA, Users' Guide for the Industrial Source Complex (ISC3) Dispersion, Environmental Protection Agency, 1995 EPA-454/B-95-003a.
- [46] O. Sutton, A theory of eddy diffusion in the atmosphere, *Proc. R. Soc. Lond. - Ser. A Contain. Pap. a Math. Phys. Character* 135 (826) (1932) 143–165, <https://doi.org/10.1098/rspa.1932.0025>.
- [47] F. Pasquill, The estimation of the dispersion of windborne material, *Meteorol. Mag.* 90 (1961) 33–49.
- [48] Á. Leelőssy, F. Molnár, F. Izsák, Á. Havasi, I. Lagzi, R. Mészáros, Dispersion modeling of air pollutants in the atmosphere: a review, *Open Geosci.* 6 (3) (2014), <https://doi.org/10.2478/s13533-012-0188-6>.
- [49] J.C. Dutton, R.E. Coverdill, Experiments to study the gaseous discharge and filling of vessels, *Int. J. Eng. Educ.* 13 (2) (1997) 123–134.
- [50] X. Guo, W. Tan, L. Liu, C. Liu, G. Zhu, Experimental study of liquefied gas dynamic leakage behavior from a pressurized vessel, *Process Saf. Environ. Protect.* 151 (2021) 20–27 <https://doi.org/10.1016/j.psep.2021.05.005>, Institution of Chemical Engineers.
- [51] D. Ahmetovic, F. Avanzini, A. Barate, C. Bernareggi, G. Galimberti, L.A. Ludovico, S. Mascetti, G. Presti, Sonification of rotation instructions to support navigation of people with visual impairment, in: 2019 IEEE Int. Conf. Pervasive Comput. Commun. PerCom 2019, 2019, <https://doi.org/10.1109/PERCOM.2019.8767407>.
- [52] G. Presti, D. Ahmetovic, M. Ducci, C. Bernareggi, L.A. Ludovico, A. Baratè, F. Avanzini, S. Mascetti, Iterative design of sonification techniques to support people with visual impairments in obstacle avoidance, *ACM Trans. Access. Comput.* 14 (4) (2021), <https://doi.org/10.1145/3470649>.
- [53] A.C. Caputo, B. Kalemi, F. Paolacci, D. Corritore, Computing resilience of process plants under Na-Tech events: methodology and application to seismic loading scenarios, *Reliab. Eng. Syst. Saf.* 195 (2020), 106685 <https://doi.org/10.1016/j.ress.2019.106685>, Elsevier Ltd.
- [54] B. Kalemi, A.C. Caputo, F. Paolacci, Resilience calculation of process plants under seismic loading: a case study, *Am. Soc. Mech. Eng. Press. Vessel. Pip. Div. PVP* (July) (2019) 5, <https://doi.org/10.1115/PVP2019-93311>.
- [55] T.D. Ancheta, R.B. Darragh, J.P. Stewart, E. Seyhan, W.J. Silva, B.S.J. Chiou, K.E. Wooddell, R.W. Graves, A.R. Kottke, D.M. Boore, T. Kishida, J.L. Donahue, NGA-West2 database, *Earthq. Spectra* 30 (3) (2014) 989–1005, <https://doi.org/10.1193/070913EQS197M>.